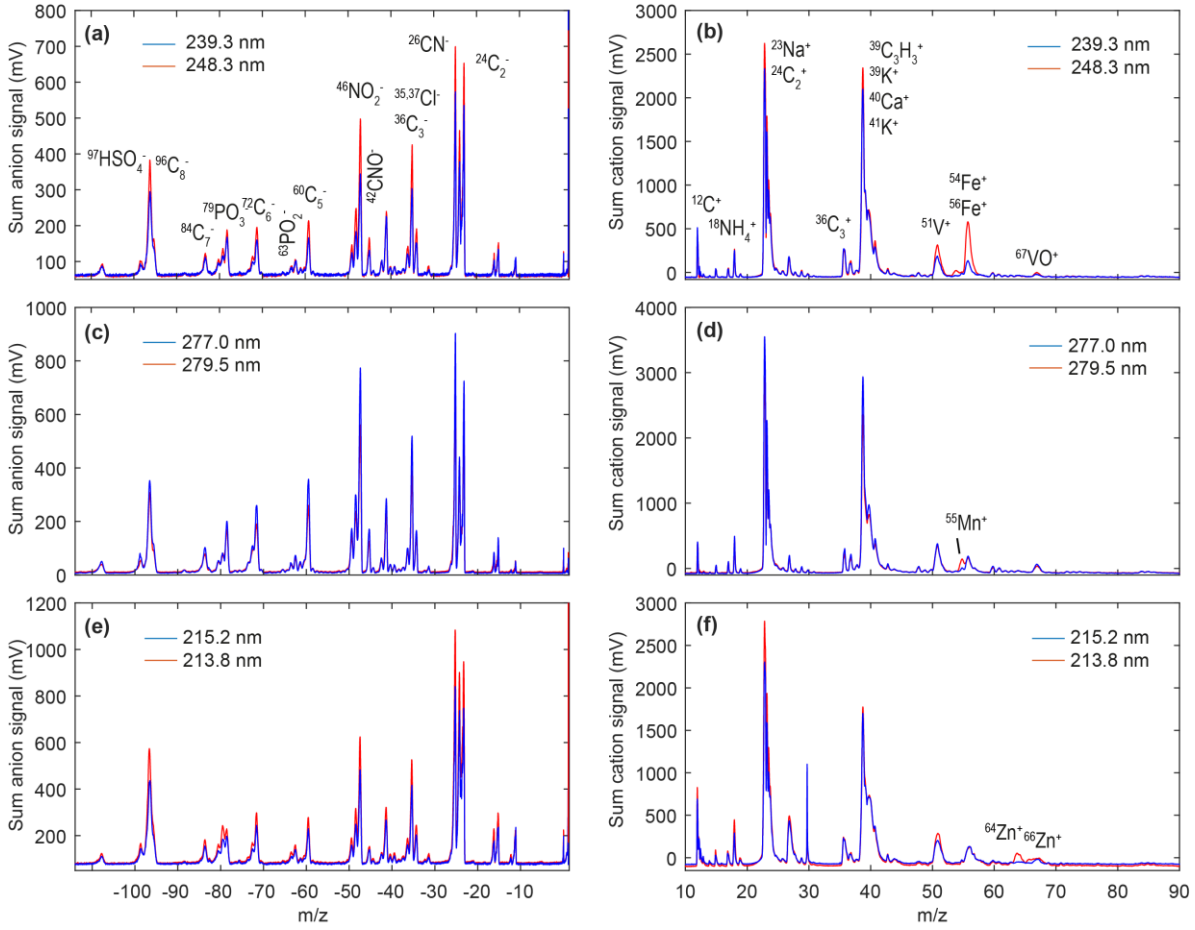

Figure S1: Accumulated mass spectra (n=400) of re-dispersed urban dust particles (Reference Material NIST 1649b), each for non-resonant (blue) and resonant (red) ionization with respect to (a,b) Fe, (c,d) Mn and (e,f) Zn. Some commonly observed ions are indicated.

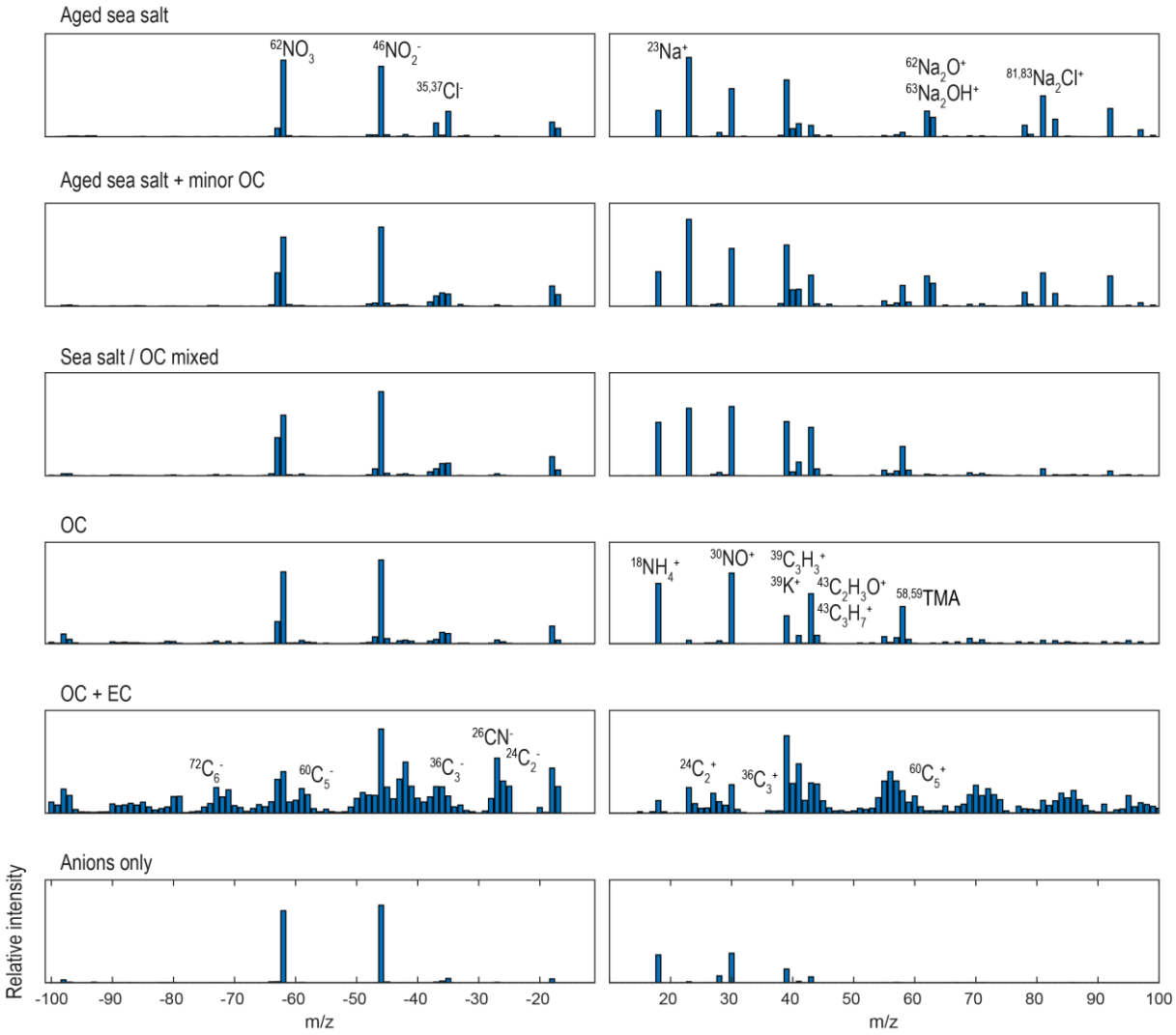

Figure S2: Main particle categories from the ambient air experiment with the 193 nm ArF laser after ART-2a clustering followed by manual merging with respect to the main compounds, see Table 2 for further details. Most particles were mixed of sea salt contributions, nitrate and organic fragments. EC signatures were detected in only 250 particles, along with strong fragment signals and partly with Fe signatures. They appeared occasionally over the full time and not within a single episode.

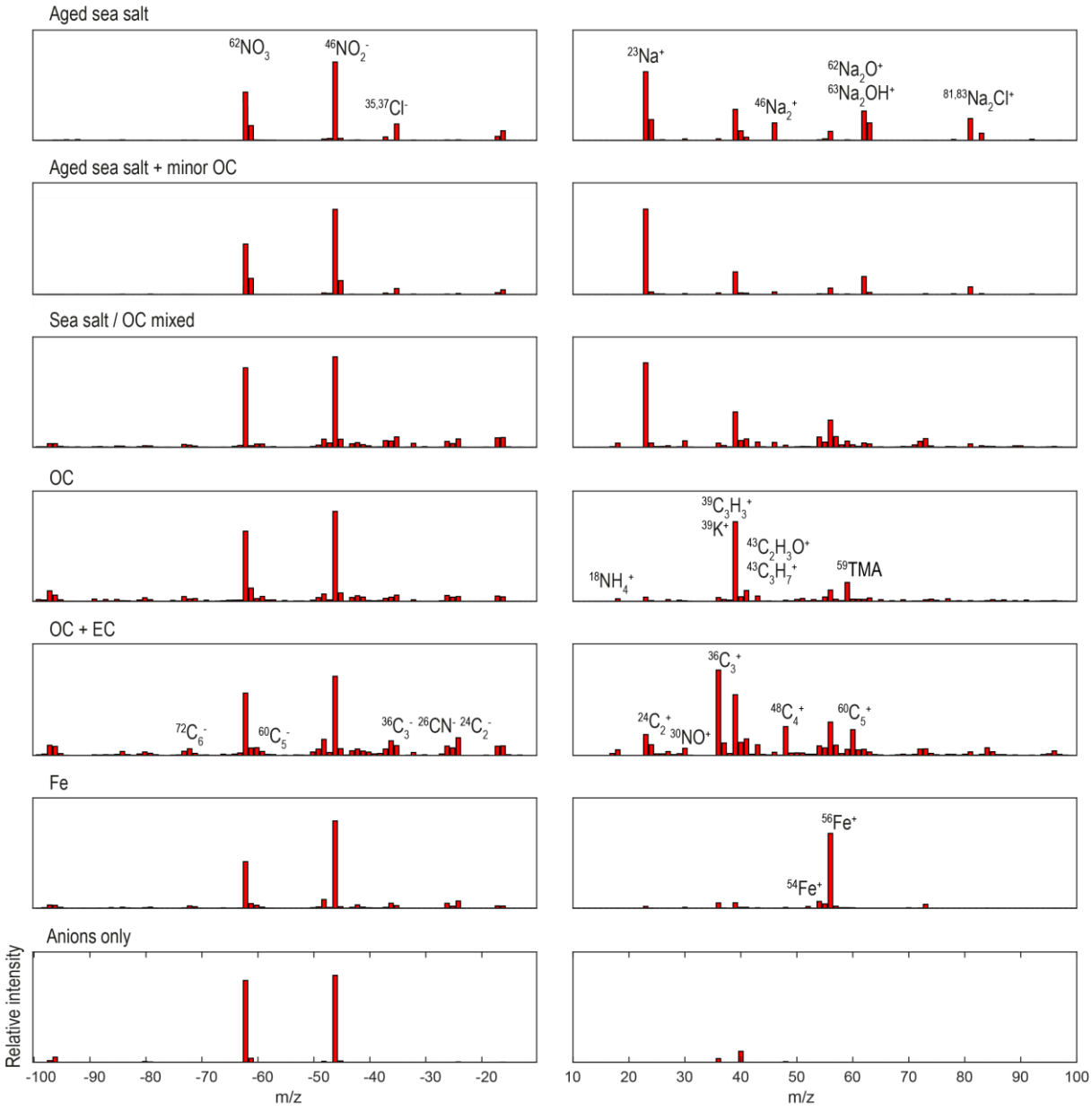

Figure S3: Main particle categories from the ambient air experiment with the 248 nm KrF laser after ART-2a clustering followed by manual merging with respect to the main compounds, see Table 2 for further details. Most particles were mixed of sea salt contributions, nitrate and organic fragments. Many particles that showed only anions (m/z=+54…56 were excluded from the ART-2a clustering) revealed exclusively Fe-signature in their cation spectra, contributing an own cluster. Fe-signatures appeared also for many particles with organic content. Differences between the two wavelengths beyond Fe-detection will be discussed in a future publication.

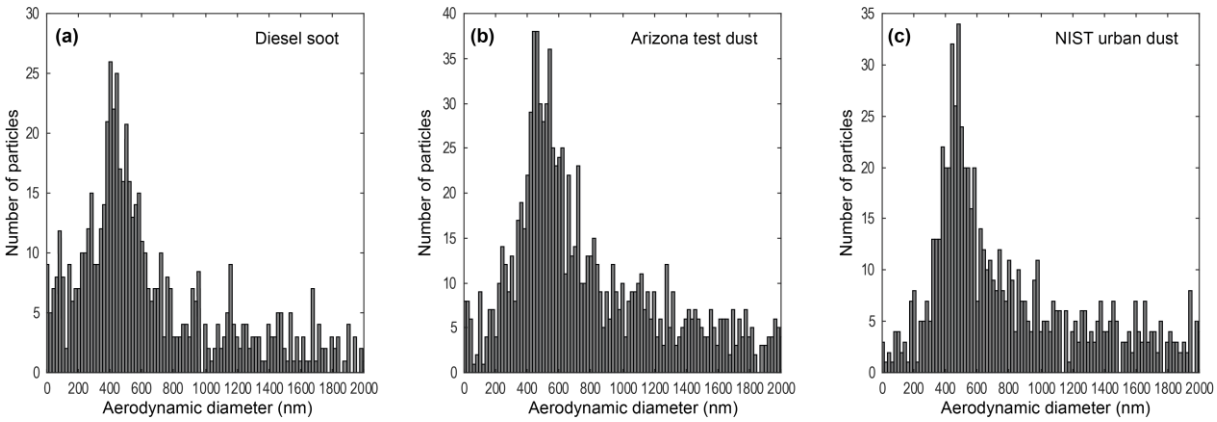

Figure S4: Particle size distributions, measured with the laser velocimetry sizing unit of the SPMS instrument. (a) Re-dispersed diesel soot particles from the car, (b) re-dispersed Arizona test dust particles, (c) re-dispersed NIST urban dust 1649b particles.

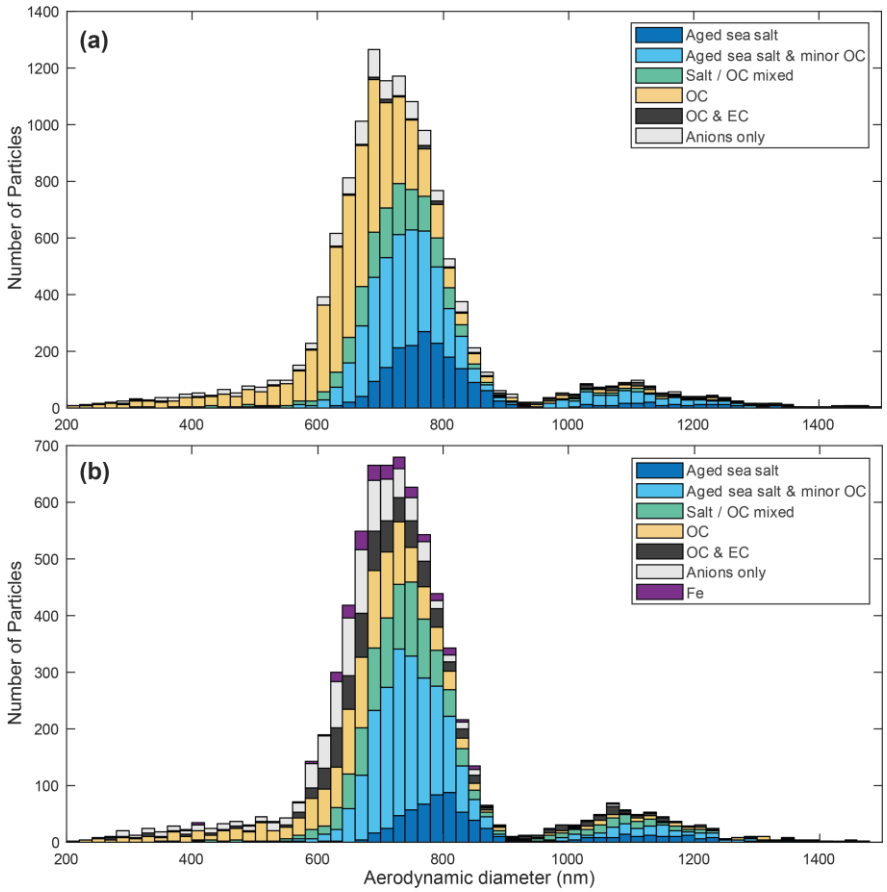

Figure S5: Particle size distribution of the main particle classes in the ambient air experiment; (a) for ionization with the 193 nm ArF-laser and (b) for the 248 nm KrF-laser. Note that the cutpoint for efficient aerosol concentration (≈0.5…1 µm), for optimum optical detection efficiency and the typical long-range transport size mode roughly coincide, thus the size distribution is rather narrow and biased by the instrument. However, it can be noticed that OC-dominated particles dominate the smaller size range while sea salt particles contribute mainly to the larger sizes and to the second mode at 1-1.2 µm.